796
doi:10.1017/S1431927622003592
Microsc. Microanal. 28 (Suppl 1), 2022

High-Speed, High-Precision, and High-Throughput Strain Mapping with Cepstral Transformed 4D-STEM Data

Dasol Yoon[1,2], Harikrishnan K.P.[1], Yu-Tsun Shao[1] and David A. Muller[1,3*]

[1.] School of Applied and Engineering Physics, Cornell University, Ithaca, NY, United States.
[2.] Department of Materials Science and Engineering, Cornell University, Ithaca, NY, United States.
[3.] Kavli Institute at Cornell for Nanoscale Science, Cornell University, Ithaca, NY, United States.
* Corresponding author: david.a.muller@cornell.edu

Strain engineering in applications such as semiconductor devices and energy conversion systems has been key to enhancing device performance [1, 2]. Here, we demonstrate fast (0.1 ms/pixel) and precise (0.1%) strain mapping by using exit wave power cepstrum (EWPC) transform [3] on datasets taken with a new 4D-STEM detector—the electron microscope pixel array detector (EMPAD)-G2 [4]. The EMPAD-G2 detector can operate at 10,000 frames per second, with single electron sensitivity and a linear response up to currents of 180 pA/pixel or more. This ensures the maximum usable imaging speed (MUIS) for high signal to noise ratio imaging remains close to the maximum frame rate, allowing maps to be recorded in seconds rather hours. With the reduced acquisition times, data processing times need to be reduced as well. The EWPC technique allows fast and memory-efficient strain mapping, and offers increased robustness to tilt and thickness artifacts. At higher doses, using precession further improves the precision by diminishing the artifacts from dynamical diffraction contrast.

The schematic of a typical 4D-STEM experiment and the EWPC processing steps are shown in Fig. 1. Individual diffraction patterns recorded for each scan position, and the log of each pattern is Fourier transformed to produce the cepstral pattern. The peaks in the EWPC pattern correspond to projected interatomic distances in the crystal and their positions can be measured with sub-pixel precision to measure the strain. Precision in EWPC depends on dose and the largest collected angle, rather than the number of pixels on the detector, making it well-suited to the EMPAD design.

Strain maps of the silicon wedge sample over large field of view are shown in Fig. 2 to compare different strain mapping algorithm's performance in the presence of thickness variations. Fig. 2(b-d) show strain maps obtained from the same 4D dataset (1 mrad semi-convergence angle (α) and 1 pC dose) with EWPC, py4DSTEM, and center of mass (CoM) methods, respectively. Ideally, the corresponding strain map should not show thickness fringes, but rather a flat, uniform distribution. Thus, the standard deviation of measured strain can describe the precision, and the mean of strain can describe the accuracy of that strain mapping method. Based on precision and accuracy with respect to thickness as shown in Fig. 3(a), CoM tends to generate low accuracy and low precision; py4DSTEM medium accuracy and medium precision; and EWPC high accuracy and high precision strain maps for EMPAD data. Note that the experimental conditions were optimized for EWPC. If the strain maps were acquired with each algorithm's optimized experimental conditions (for example, more pixels per disk for py4DSTEM method), the differences in performance between the different algorithms would likely be smaller than the differences as a function of thickness. This is to say that thickness and tilt variations between different samples still have larger variations in reproducibility on the optimized measurements than the choice of processing method.

In Fig. 3, different experimental conditions—such as dwell time, α, and beam current—are explored to determine their impacts on precision. Fig. 3(b) shows that smaller α and higher dose tend to yield higher

precision, up until the point that systematic errors from diffraction artifacts dominates over the Poisson noise. Fig. 3(c) shows the trade-off between precision and time as a function of estimated probe sizes. The probe sizes are calculated considering both diffraction limit and source size contribution.

In order to achieve higher precision strain mapping, a higher dose is required, and to get higher throughput via faster acquisition, higher beam current is needed. With the use of the EWPC transform, strain mapping of the silicon wedge yielded precision of 0.1% at dose of 1 pC and α of 1 mrad. The high current range of the EMPAD-G2 makes it possible to record this dose in a ms or less, depending on the gun brightness [5].

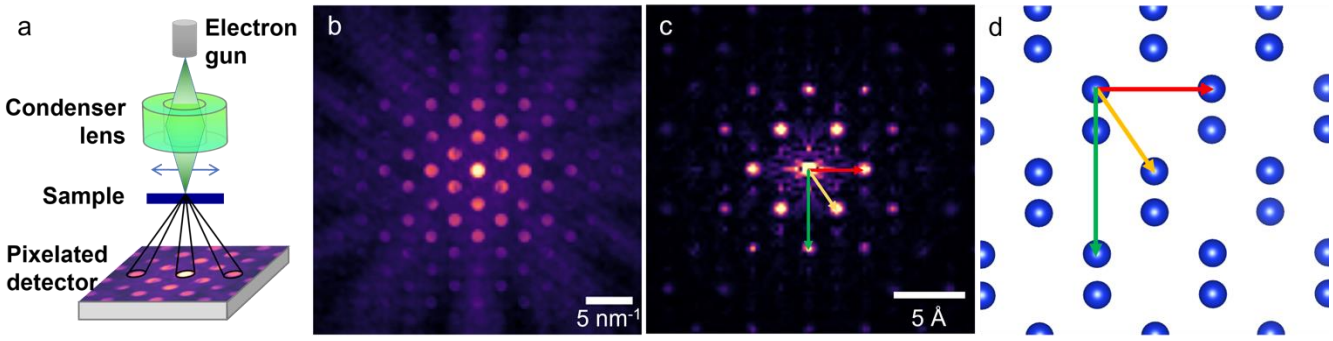

Figure 1. Illustration of exit wave power cepstrum (EWPC) transform. (a) Schematic of 4D-STEM. (b) Simulated position averaged convergent beam diffraction (PACBED) pattern of 30 nm thick Si [110] shown on a logarithmic scale. (c) EWPC transform of (b) shown on a logarithmic scale. (d) Structural model of Si [110]. Colored arrows indicate projected inter-atomic distances, and corresponding peaks in EWPC are shown in (c) with matching colors (red: 3.84 Å; yellow: 3.33 Å; green: 5.43 Å).

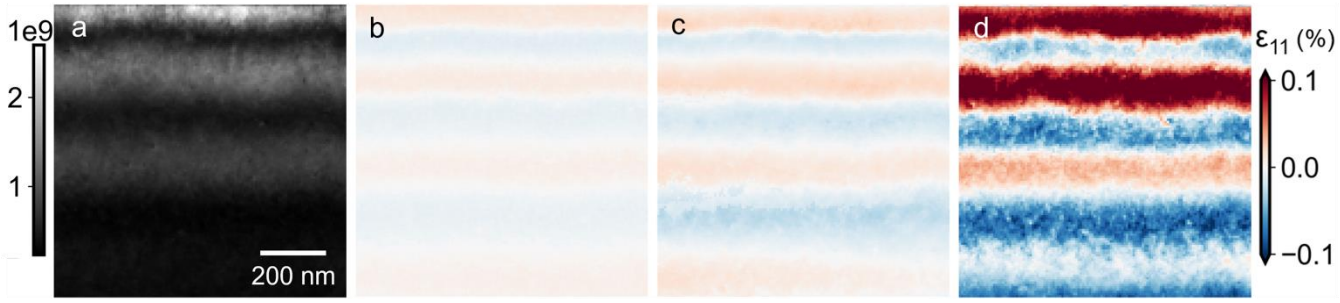

Figure 2. Different strain mapping methods applied to the same 4D dataset of a Si [110] wedge. The thickness of the wedge gets gradually thicker towards the bottom of the figure. (a) Virtual dark field image of the wedge created with (1-1 1) Bragg spot. Corresponding strain maps calculated using the (b) EWPC, (c) py4DSTEM, and (d) center of mass (CoM) methods. The measured precision with EWPC is 2x better than that of py4DSTEM and 10x better than CoM for this EMPAD data set.

https://doi.org/10.1017/S1431927622003592 Published online by Cambridge University Press

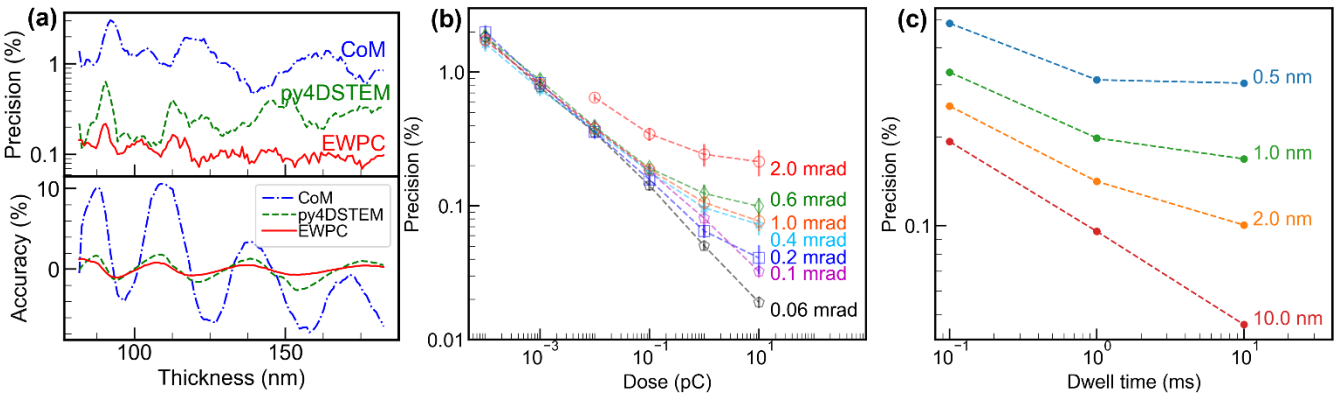

Figure 3. Local precision of EWPC strain maps acquired with varying experimental conditions. (a) Precision and accuracy of each strain mapping method as a function of thickness, showing EWPC method's robustness to thickness artifacts compared to other processing methods for the same data set from figure 2. Log-log plots of EWPC precision as a function of (b) dose for different probe semi-convergence angles (c) dwell time for different estimated probe sizes, where both diffraction limit and source size contribution are taken into account.

References:

[1] Z Peng et al., Light Sci Appl **9** (2020), p. 190. doi: 10.1038/s41377-020-00421-5
[2] D Schlom et al., MRS Bulletin **39** (2014), p. 118. doi: 10.1557/mrs.2014.1
[3] E Padgett et al., Ultramicroscopy **214** (2020), p. 112994. doi: 10.1016/j.ultramic.2020.112994
[4] HT Philipp et al., arXiv:2111.05889 [physics.ins-det] (2021)

[5] Work primarily supported by the Center for Alkaline Based Energy Solutions (CABES), a DOE EFRC BES award # DE-SC0019445. Facilities supported by the National Science Foundation (DMR-1429155, DMR- 2039380, DMR-1719875)